Piezomechanics Using Intelligent Variable-Structure Control

Chih-Lyang Hwang, Chau Jan, and Ye-Hwa Chen

***Abstract*—The so-called piezomechanics contain three parts: piezoelectric translator, carriage mechanism, and control system. It is well known that piezomechanics have three drawbacks: 1) it should only be loaded axially; 2) it contains a hysteresis feature; and 3) its expansion is dependent on temperature. The first drawback is tackled by the design of the carriage mechanism. This paper focuses on dealing with the second and third drawbacks by using an intelligent variable-structure control. First, a neural network is employed to learn the dynamics of the piezomechanism. Second, a novel forward control based on the learned model is employed to achieve an acceptable tracking result. Because the tracking performance by a forward control cannot be guaranteed as the system is subject to uncertainties, a discrete-time variable-structure control is synthesized to improve the performance. No state estimator is required for the proposed control. The stability of the overall system is verified via the Lyapunov analysis. Experiments are also presented to confirm the effectiveness of the proposed control.**

***Index Terms*—Discrete-time variable-structure control, neural-network modeling, piezomechanics.**

I. Introduction

DUE TO THE requirements of nanometer resolution in displacement, high stiffness, and fast frequency response, there are many precision positioning applications using piezoelectric actuators, e.g., scanning tunneling microscopy [1], active vibration control of rotor bearing systems [2], diamond turning machines [3], and piezoelectric voltage feedback for grinding tables [4]. Recent advances in the development and application of materials with high piezoelectric or magneto-electric properties have extended to the area of mechanics. The so-called piezomechanics include three parts: piezoelectric translator, carriage mechanism, and control system [5]. It is well known that a piezoelectric translator possesses the following advantageous features [1]–[11]: 1) unlimited resolution—it is possible to make extremely fine positional changes in the nanometer (i.e., 10^{-9} meter) range; 2) no moving parts—its expansion is based on a purely solid-state deformation and shows no sign of aging; 3) high efficiency—the piezo effect directly converts electrical energy into a linear movement; 4) large forces—masses of more than 10 t can be moved and positioned accurately within nanometers by a single piezo actuator; and 5) fast response—its expansion speed is only limited by the speed of sound in the ceramic material. However, it also has the following disadvantageous characteristics: 1) it should only be loaded axially; 2) its expansion is not proportional to the electric field strength—its nonlinear behavior is shown by a hysteresis curve; and 3) the stringent requirement of positioning accuracy must consider the effect of temperature.

To cope with the first drawback, an effective mechanism design must be used to avoid (or at least reduce) the effect of loads other than axial ones. This paper proposes to address the second and third drawbacks. The reasons are as follows. Because the hysteresis is not a differentiable and one-to-one nonlinear mapping, it is often unknown. It also severely limits the system performance via, e.g., undesirable oscillation or instability [1]–[11]. The way for an effective controller for the system with hysteresis is, therefore, important. Recently, Tao and Kokotovic [9] used a simplified hysteresis model to capture certain hysteresis features. Then, an adaptive hysteresis inverse cascades with the system to cancel the effect of hysteresis so that the remaining part of system becomes a linear structure with uncertainties. Furthermore, a paper developed by Ge and Jouaneh [10] discusses a comparison between a feedforward control, a regular proportional–integral–derivative (PID) control, and a PID feedback control with hysteresis modeling in the feedforward loop. Their results show that the tracking control is greatly improved by augmenting the feedback loop with a model of hysteresis in the feedforward loop. However, the result is only valid for tracking cyclic reference signals.

In this paper, a novel neural-network model, which includes two different nonlinear gains according to change rate of input signal and a linear dynamic system, is employed to learn the piezomechanism [12]. It is the first time to model a nondifferentiable and not one-to-one nonlinear mapping dynamic system. The feature is not obtained by using the traditional neural-network modeling because of its approximation for a differentiable and one-to-one nonlinear mapping. A new forward control based on the learned neural-network model is used to achieve an acceptable tracking performance. The proposed forward control includes a reinforcement to reduce the discontinuity of hysteresis. The tracking performance using a forward control cannot be assured as the system is subject to temperature variations or external load, or the aging of system components. Then, the second procedure of the proposed intelligent variable-structure control (IVSC) is to construct a discrete-time variable-structure control (DVSC) to improve the system performance. Variable-structure control (VSC) design possesses the advantages of a fast response without overshoot and good performance in the presence of parameter

Manuscript received August 20, 1998; revised October 14, 2000. Abstract published on the Internet November 15, 2000. The work of C.-L. Hwang and C. Jan was supported in part by the National Science Council of R.O.C. under Grant NSC-88-2212-E-036-0007.

C.-L. Hwang and C. Jan are with the Department of Mechanical Engineering, Tatung University, Taipei 10451, Taiwan, R.O.C.

Y.-H. Chen is with the George W. Woodruff School of Mechanical Engineering, Georgia Institute of Technology, Atlanta, GA 30332-0405 USA.

Publisher Item Identifier S 0278-0046(01)01118-2.

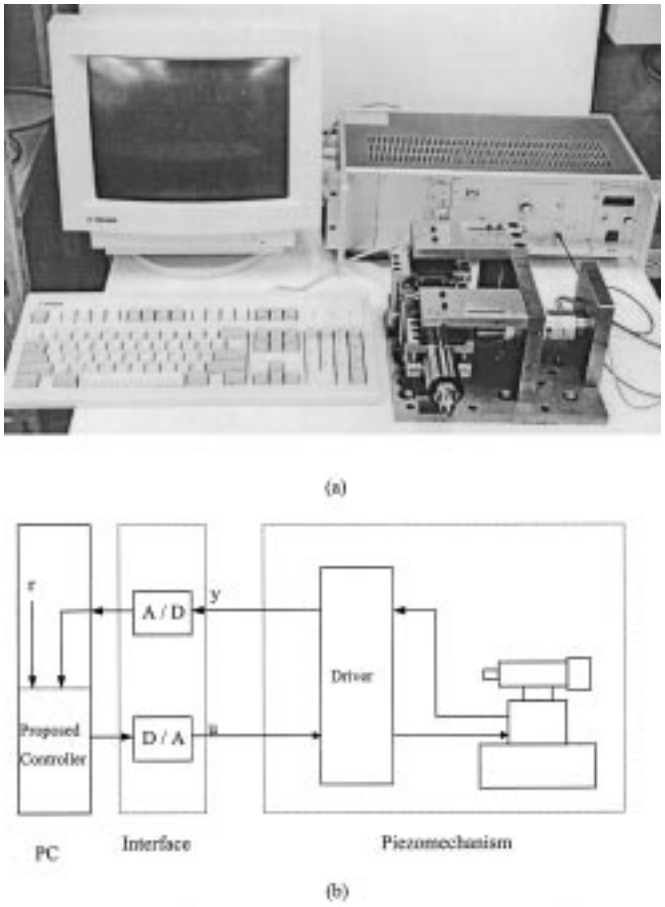

Fig. 1. Experimental setup of the overall system. (a) Photograph. (b) Control block diagram.

variations [13]–[22]. However, traditional VSC always results in chattering because of its discontinuous switching feature. Fortunately, the first procedure of the proposed controller captures the dominant features of piezomechanics. The system uncertainties are, thus, reduced. Furthermore, the switching part of DVSC is small so that the occurrence of chattering control input becomes small. This characteristic is the so-called "intelligent" VSC.

II. Experimental Setup

The piezomechanics consist of three parts: piezotranslator (including position sensor and driver), carriage mechanism, and control system (including AD/DA card, 80586 personal computer, and DVSC program). The block diagram of the experimental setup is shown in Fig. 1. The carriage mechanism is made of steel for enhancing the strength of the mechanism. Four linear guides provided by THK Company(model number VRU3088) are used to support the moving part of the mechanism. Furthermore, a high-speed spindle with weight of 3.5 kg (model number PRECISE 3040) is fixed on the carriage mechanism. The piezotranslator is a model number P-246.70 from Physical Instrument (PI) Company. Its specifications are briefly described as follows: maximum expansion 120 μm, electric capacitance 3000 nF, stiffness 190 N/μm, resonant frequency 3.5 kHz, and temperature expansion 2 μm/K. The position signal is achieved by a position sensor model number P-177.10 of PI Company. The

TABLE I
Maximum Tracking Error (μm) for the Reference with Amplitude 36 μm and Various Frequencies (the Superscription 1 and 2 of Forward and Proposed Control Denote the Tracking Result Based on Identified Model with 15- and 25-Hz Input, Respectively)

Controller \ Frequency (Hz)	5	10	15	20	25	30	40
Open System Response	4.89	4.97	4.86	5.29	5.68	5.79	6.08
PID Control	3.67	3.17	2.77	2.37	2.09	2.74	2.98
Forward Control^1	3.78	2.77	1.59	1.66	2.01	2.48	3.09
Proposed Control^1	1.87	1.37	0.79	0.97	1.08	1.47	1.69
Forward Control^2	3.92	2.82	1.82	1.67	1.52	1.74	2.73
Proposed Control^2	1.95	1.46	1.05	0.98	0.73	1.02	1.51

TABLE II
Magnitude (dB) and Phase (Degree) of Frequency Response

Controller \ Frequency (Hz)		5	10	15	20	25	30	40
Open System Response	dB	-1.26	-1.29	-1.20	-1.38	-1.49	-1.52	-1.60
	degree	-14.4	-15.8	-17.2	-17.28	-18.1	-17.3	-15.5
PID Control	dB	-0.93	-0.80	-0.69	-0.59	-0.52	-0.69	-0.75
	degree	-8.64	-11.52	-9.59	-11.22	-13.5	-12.96	-14.2
Proposed Control	dB	-0.463	-0.337	-0.193	-0.24	-0.26	-0.37	-0.43
	degree	-2.16	-2.88	-1.98	-3.02	-2.52	-2.98	-2.72

signal is received by a 14-bit A/D card (PCL-814) in an 80586 personal computer. After sampling by the A/D card, the resolution of the true position is 0.007 μm. Together with a reference input in the computer program written by Turbo C, the control signal $u(k)$ is calculated. The control input through the D/A card is then sent to the driver which is a model number of P-271.10 from PI Company. The output signal of driver with voltage between -200 and 1000 V is employed to drive the piezotranslator. The different position signal is accomplished by using a different input signal. The process is repeated until the total process time is over. The time required for every process is called the "control cycle time (T_c)."

III. System Analysis and Modling

A. System Analysis

The sinusoidal responses with amplitude 36 μm and various frequencies of 5, 15, 25, 40, and 50 Hz, are shown in Fig. 2 or the first rows of Tables I and II. From Fig. 2 or Tables I and II, the tracking error (i.e., $u - y$) increases as the frequency of input u increases. Furthermore, the phase shift between the input u and the output y increases as the frequency of input u increases. The tracking error for the open-loop system is over

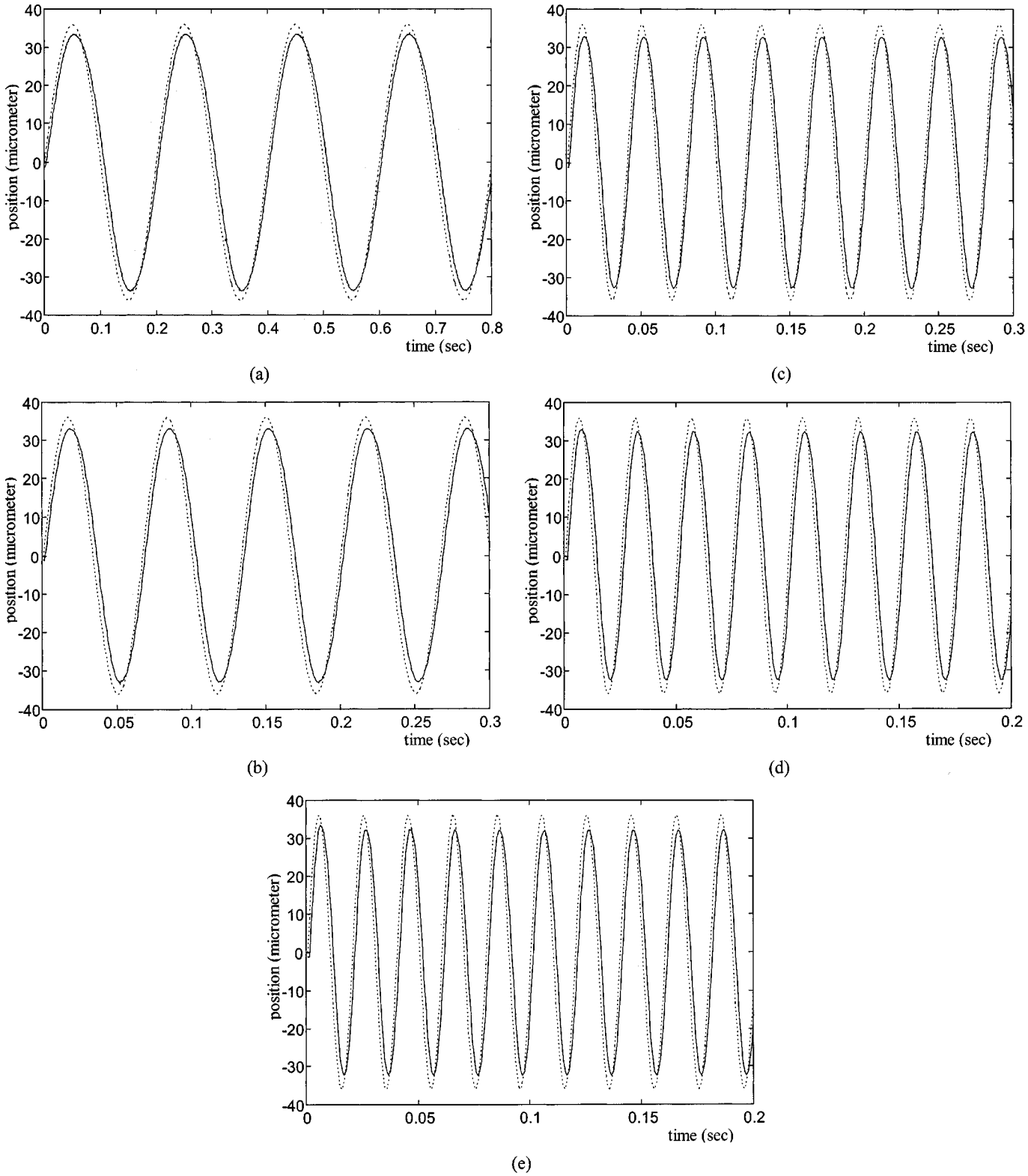

Fig. 2. Time histories of output responses (—) of open-loop system for various reference $36\sin(2\pi ft)$ μm (. . .). (a) f = 5 Hz. (b) f = 15 Hz. (c) f = 25 Hz. (d) f = 40 Hz. (e) f = 50 Hz.

14% of the amplitude of input. These tracking results are not acceptable for the precise positioning. The main reason for this result is the hysteresis phenomenon of piezomechanism. Fig. 3 indicates the output responses of the piezomechanism for an increasing input and a decreasing input. The maximum error due to hysteresis can be as much as 10%–15% of the path covered if the piezomechanism is run in an open-loop system. Under the circumstances, an effective controller is needed to improve the tracking performance. Only in Fig. 3 has applied positive input voltage been used to achieve the positive position signal. The other figures possess bipolar output and input signals by using the adjustment of hardware and software.

B. System Modeling

Throughout this paper, a polynomial representation is defined as $A(q^{-1}) = a_0 + a_1 q^{-1} + \cdots + a_{n_a} q^{-n_a}$, where a_i for $i = 0, 1, \cdots, n_a$ denote bounded coefficients, n_a stands for the system degree (i.e., if $a_{n_a} \neq 0$, deg $\{A(q^{-1})\} = n_a$), and q^{-1} denotes the backward-time-shift operator [i.e., $q^{-1}y(k) \equiv y(k-1)$]. Based on the system sinusoidal responses in Fig. 2 and the effect of hysteresis analysis in Fig. 3, the following neural-network model is proposed:

$$y_n(k) = -\sum_{i=1}^{m} a_i(k-1)y(k-i) + \sum_{i=1}^{m} b_i(k-1)v(k-i) \tag{1}$$

$$v(k) = N(u, c_1, c_2, c_3) = \frac{1 + c_1(k)c_3(k) - z(k)}{c_1(k)[1 + z(k)]} \tag{2}$$

where

$$z(k) = e^{-2c_1(k)[u(k) - c_2(k)]} \tag{3}$$

the weights $a_i(k), b_i(k)(1 \leq i \leq m)$, and $c_j(k)(1 \leq j \leq 3)$ are adjusted by an offline learning scheme [12]. Because the proposed piezomechanism contains the hysteresis feature, two nonlinear functions in (2) according to the change rate of $u(k-1)$, i.e., $\Delta u(k-1) = u(k-1) - u(k-2)$, are used to approximate the hysteresis, which is not a one-to-one and continuously differentiable mapping. An optimal model to approximate the dynamics of piezomechanism is described as follows:

$$a_i(k) = \overline{a}_i \quad b_i(k) = \overline{b}_i, \qquad 1 \leq i \leq m \tag{4}$$

$$c_j(k) = \begin{cases} \overline{c}_{pj} & \text{as } \Delta u(k-1) \geq 0 \\ \overline{c}_{nj} & \text{as } \Delta u(k-1) < 0 \end{cases} \qquad 1 \leq j \leq 3 \tag{5}$$

where $\overline{a}_j, \overline{b}_j (1 \leq j \leq m)$ and $\overline{c}_{pj}, \overline{c}_{nj} (1 \leq j \leq 3)$ are not necessarily unique. The following cost function is defined to the learning process:

$$J(k) = e_r^2(k)/2 \tag{6}$$

where $e_r(k) = y_p(k) - y_n(k)$ and $y_p(k)$ denotes the output of the piezomechanism. The gradient learning law for the cost function (6) is expressed as follows:

$$a_i(k) = a_k(k-1) - \alpha_i(e_r)\frac{\partial J(k)}{\partial a_i(k-1)}, \qquad 1 \leq i \leq m \tag{7a}$$

$$b_i(k) = b_i(k-1) - \beta_i(e_r)\frac{\partial J(k)}{\partial b_i(k-1)}, \qquad 1 \leq i \leq m \tag{7b}$$

$$c_j(k) = c_j(k-1) - \gamma_j(e_r)\frac{\partial J(k)}{\partial c_j(k-1)}, \qquad 1 \leq j \leq 3 \tag{7c}$$

where the partial derivatives and time-varying learning gains are described in Appendix A. The typical coefficients of time-varying learning gains with $\zeta_i = 0.5$ and $\delta_i = \rho_i = 0.1$ are used.

After an effective learning and a model verification (see Fig. 4), a suitable order of piezomechanism (i.e., m) is selected to be three. The 12 weightings are given in Appendix B.

Remark 1: During the offline learning, the input signal $36\sin(30\pi t)$ μm is employed to achieve two nonlinear gains with six coefficients in (5) and a set of coefficients in (4).

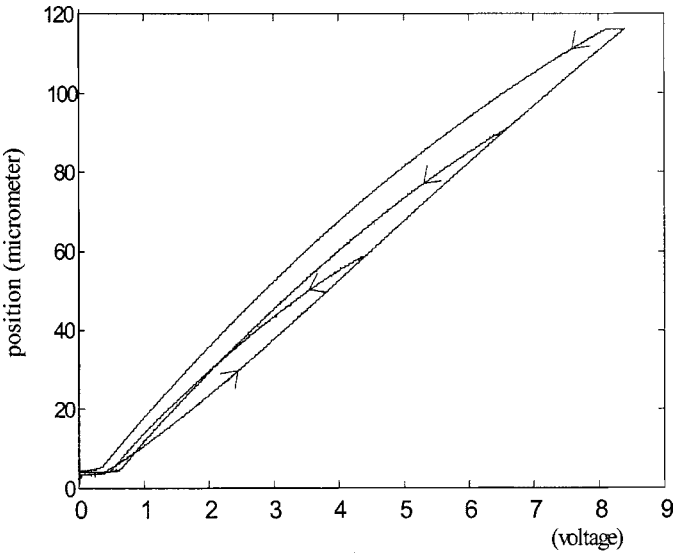

Fig. 3. Hysteresis characteristic.

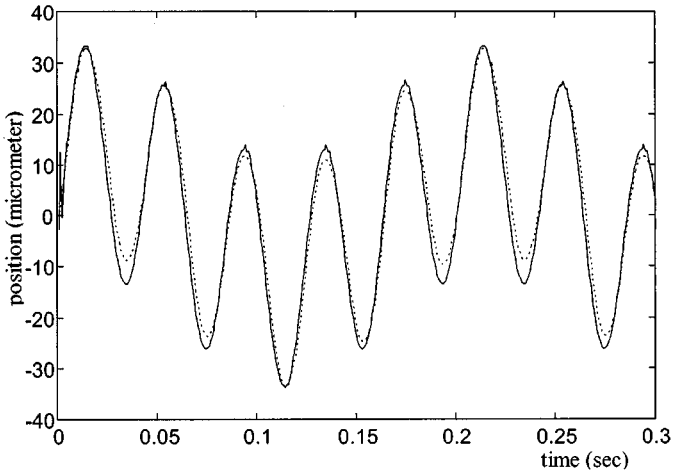

Fig. 4. Time histories of output responses of piezomechanics $(\ldots)$ and mathematical model (—) for $u(t) = 24\sin(50\pi t) + 12\sin(10\pi t)$ μm.

Because only a set of coefficients $\overline{a}_i, \overline{b}_i (1 \leq i \leq m)$ are obtained, a set of coefficients $\overline{a}_i, \overline{b}_i (1 \leq i \leq m)$ must satisfy two different behaviors of hysteresis and are described as the following steps.

1) A set of coefficients $\overline{a}_i, \overline{b}_i (1 \leq i \leq m)$ and $\overline{c}_{pj} (1 \leq j \leq 3)$ with a monotonically increased input signal is learned.
2) The coefficients are set to be the initial values for the learning of $\overline{a}_i, \overline{b}_i (1 \leq i \leq m)$ and $\overline{c}_{nj} (1 \leq j \leq 3)$ with a monotonically decreased input signal. Under this circumstance, the learning rate $\alpha_i(e_r), \beta_i(e_r)$ in (7a), (7b) must be small to let $\overline{a}_i, \overline{b}_i (1 \leq i \leq m)$ change small.
3) The coefficients $\overline{a}_i, \overline{b}_i (1 \leq i \leq m)$ obtained by step 2) are assigned to be the initial values for the modification of $\overline{c}_{pj} (1 \leq j \leq 3)$ with a monotonically increased input signal and learning rate $\alpha_i(e_r) = \beta_i(e_r) = 0$, but $\gamma_j(e_r) \neq 0$ in (7c).
4) Two sets of different nonlinear coefficients $\overline{c}_{pj}$ and $\overline{c}_{nj} (1 \leq j \leq 3)$ and a set of coefficients $\overline{a}_i, \overline{b}_i (1 \leq i \leq m)$ are achieved to approximate the hysteresis characteristic.

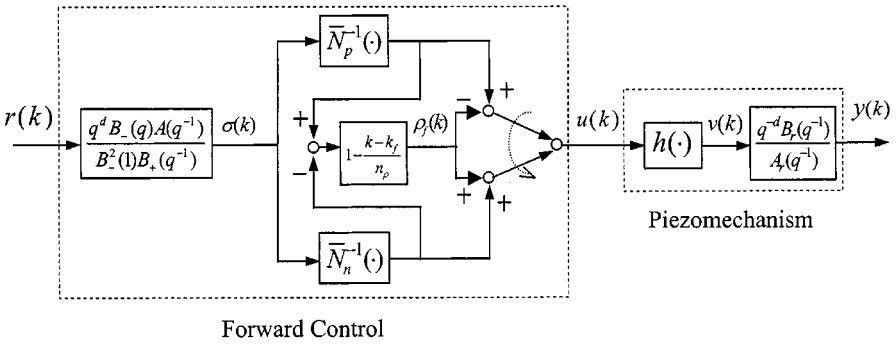

Fig. 5. Block diagram of forward control.

Hence, the dynamics of nominal piezomechanism are given as follows:

$$A(q^{-1})y(k) = q^{-d}B(q^{-1})v(k) \tag{8}$$

$$v(k) = \overline{N}[u(k)] \tag{9}$$

where $d = 1, a_0 = 1, a_i = \overline{a}_i, b_{i-1}$ for $i = 1, 2, 3$, and

$$\overline{N}[u(k)] = \begin{cases} \overline{N}_p[u(k)] = \dfrac{1 + \overline{c}_{1p}\overline{c}_{3p} - \overline{z}_p(k)}{\overline{c}_{1p}[1 + \overline{z}_p(k)]}, \\ \quad \text{if } \Delta u(k-1) \geq 0 \\ \overline{N}_n[u(k)] = \dfrac{1 + \overline{c}_{1n}\overline{c}_{3n} - \overline{z}_n(k)}{\overline{c}_{1n}[1 + \overline{z}_n(k)]}, \\ \quad \text{if } \Delta u(k-1) < 0 \end{cases} \tag{10a}$$

$$\overline{z}_p(k) = e^{-2\overline{c}_{1p}[u(k) - \overline{c}_{2p}]}; \quad \overline{z}_n(k) = e^{-2\overline{c}_{1n}[u(k) - \overline{c}_{2n}]}. \tag{10b}$$

Furthermore, $A(q^{-1})$ is a stable matrix.

IV. Controller Design

We first determine a forward control based on the 12 weightings of the neural-network model. Then, an adaptation from a DVSC is combined with the previous forward control to improve the system performance.

A. Forward Control

After an effective learning, the nonlinear function in (9) becomes a function of $u(k)$ only. Its inverse function $\overline{N}^{-1}[u(k)]$ for positive and negative $\Delta u(k-1)$ is described as follows:

$$\overline{N}_p^{-1}(\sigma) = \overline{c}_{2p} - \frac{1}{2\overline{c}_{1p}} \log\left[\frac{1 + \overline{c}_{1p}\overline{c}_{3p} - \overline{c}_{1p}\sigma(k)}{1 + \overline{c}_{1p}\sigma(k)}\right], \quad \Delta u(k-1) \geq 0 \tag{11}$$

$$\overline{N}_n^{-1}(\sigma) = \overline{c}_{2n} - \frac{1}{2\overline{c}_{1n}} \log\left[\frac{1 + \overline{c}_{1n}\overline{c}_{3n} - \overline{c}_{1n}\sigma(k)}{1 + \overline{c}_{1n}\sigma(k)}\right], \quad \Delta u(k-1) < 0 \tag{12}$$

where $\sigma(k)$ denotes an input signal of $\overline{N}^{-1}(\cdot)$. Certainly, the input signal $\sigma(k)$ of $\overline{N}^{-1}(\cdot)$ must satisfy the inequality $[1 + \overline{c}_1\overline{c}_3 - \overline{c}_1\sigma(k)]/[1 + \overline{c}_1\sigma(k)] > 0\ \forall k$. Based on the concept of inverse control [12] and the compensation of the discontinuity in hysteresis model, the following novel forward control (see Fig. 5) is employed to track a reference input (or desired trajectory) $r(k)$:

$$u(k) = \begin{cases} \overline{N}_p^{-1}(\sigma) - \rho_f(k), & \Delta u(k-1) \geq 0 \\ \overline{N}_n^{-1}(\sigma) + \rho_f(k), & \Delta u(k-1) < 0 \end{cases} \tag{13}$$

$$\rho_f(k) = \begin{cases} (\overline{N}_p^{-1}(\sigma) - \overline{N}_n^{-1}(\sigma))[1 - (k - k_f)/n_\rho], \\ \quad k_f \leq k \leq k_f + n_\rho \\ 0, \quad \text{otherwise} \end{cases} \tag{14}$$

where k_f is defined as the time k that $\text{sgn}[\Delta u(k-2)] \neq \text{sgn}[\Delta u(k-1)]$ and the input signal of $\overline{N}^{-1}(\cdot)$ is defined as follows:

$$\sigma(k) = q^d B_-(q)A(q^{-1})r(k)/[B_-^2(1)B_+(q^{-1})]. \tag{15}$$

As the discontinuity of nonlinear model (10) is large, n_ρ is chosen as a large integer. That is, a reinforcement $\rho_f(k)$ in (13) is employed to reduce the hysteresis error caused by the discontinuity of (10). The relation between $r(k)$ and $y(k)$ becomes

$$y(k) = q^{-d}B_r(q^{-1})[\sigma(k) - \Delta(u)]/A_r(q^{-1}) \tag{16}$$

with

$$\Delta(u) = \begin{cases} \overline{N}_p(u + \rho_f(k)) - h(u), & \Delta u(k-1) \geq 0 \\ \overline{N}_n(u - \rho_f(k)) - h(u), & \Delta u(k-1) < 0 \end{cases} \tag{17}$$

where $h(\cdot)$ denotes an unknown hysteresis of the proposed system (see Fig. 3), and $q^{-d}B_r(q^{-1})/A_r(q^{-1})$ represents an unknown linear dynamics of real piezomechanism. Before discussing the controller design, the following assumption about the approximation error of hysteresis is made:

A1: $\Delta(u) = \mu_0 + \mu_1 u(k)$, where μ_0 and μ_1 are known. (18)

Remark 2: If $\mu_0 = \mu_1 = 0$, $B_r(q^{-1}) = B(q^{-1})$ and $A_r(q^{-1}) = A(q^{-1})$, the system output $y(k)$ can track $r(k)$ in the sense of zero-phase manner for dc signal. The following section will derive a DVSC to improve the tracking error.

B. DVSC

1) Error Model Resulting From Forward Control: To compensate the tracking error caused by the forward control, a DVSC is used to combine with the previous forward control

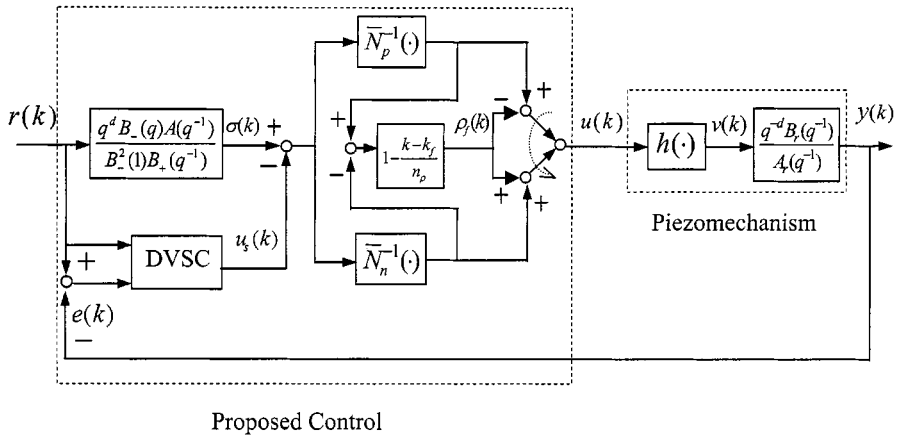

Fig. 6. Block diagram of proposed control.

(see Fig. 6). The error model of the closed-loop system in Fig. 6 is as follows:

$$A_r(q^{-1})[e(k)-e_f(k)] = B_r(q^{-1})[u_s(k-d) + \Delta(u(k-d))] \quad (19)$$

where

$$e(k) = r(k) - y(k) \quad (20)$$

$$e_f(k) = [A_r(q^{-1})B_-^2(1)B_+(q^{-1}) - B_r(q^{-1})B_-(q)A(q^{-1})]r(k)/ \cdot [A_r(q^{-1})B_-^2(1)B_+(q^{-1})]. \quad (21)$$

The notation $e_f(k)$ denotes tracking error caused by forward control, and $\Delta(u(k-d))$ denotes the uncertainties caused by the hysteresis. The subsequent work is to design a DVSC $u_s(k-d+1)$ so that $e(k)$ is as small as possible under the uncertainties $\Delta(u(k-d+1))$ and the unknown polynomials $A_r(q^{-1})$ and $B_r(q^{-1})$. First, one rewrites (19) in a state-space form

$$X(k+1) = (\overline{F}+\Delta F)X(k) + (\overline{G}+\Delta G) \cdot [u_s(k-d+1) + \Delta(u(k-d+1))] \quad (22)$$

$$e(k) = (\overline{H}+\Delta H)X(k) + e_f(k) \quad (23)$$

where the triplex $(\overline{F},\overline{G},\overline{H})$ corresponds to the nominal system of (16) which is known, observable, and controllable, and the triplex $[\Delta F, \Delta G, \Delta H]$ corresponds to the uncertainties or parameter variations of (16). In addition, $(\overline{H}+\Delta H) \neq 0$. For example, the nominal system of (22), (23) can be written as the following observable canonical form:

$$\overline{F} = \begin{bmatrix} -a_1 & 1 & & \\ \cdot & & \cdot & \\ \cdot & & & \cdot \\ \cdot & & & 1 \\ -a_n & & & 0 \end{bmatrix}$$

$$\overline{G} = \begin{bmatrix} b_0 \\ b_1 \\ \cdot \\ \cdot \\ b_{n-1} \end{bmatrix}$$

$$\overline{H} = [1 \quad 0 \quad \cdots \quad 0] \quad (24)$$

where $n = \max[n_a, n_b + d - 1]$. The system state can be represented by the combination of $e(k), \cdots, e(k-n+1)$, $u_s(k-d), \cdots, u_s(k-n-d)$ and the uncertainties $[\Delta F, \Delta G, \Delta H]$, $\Delta(u(k-d+1))$ and $e_f(k)$, i.e.,

$$x_1(k) = (1 - \Delta H H^p)[e(k) - e_f(k)] \quad (25a)$$

$$x_i(k+1) = -a_i e(k) + b_{i-1}u_s(k-d+1) + x_{i+1}(k) + \Delta\rho_i(k), x_{n+1}(k) = 0, \qquad 2 \le i \le n \quad (25b)$$

where

$$\Delta\rho_i(k) = -\Delta a_i(1-\Delta H H^p)[e(k)-e_f(k)] + a_i[\Delta H H^p e(k) + (1-\Delta H H^p)e_f(k)] + [b_{i-1}+\Delta b_{i-1}]\Delta(u(k-d+1)) + \Delta b_{i-1}u_s(k-d+1) \quad (25c)$$

$$H^p = (\overline{H}+\Delta H)^T\{(\overline{H}+\Delta H)(\overline{H}+\Delta H)^T\}^{-1}. \quad (25d)$$

Because $(\overline{H}+\Delta H) \neq 0$, the scalar $(\overline{H}+\Delta H)(\overline{H}+\Delta H)^T \neq 0$ and then H^p exists. Substituting the right-hand side of (25b) into its left-hand side and continuing the process until the index i is greater than $n-1$ yields

$$x_j(k+1) = -\sum_{i=0}^{n-j}\{a_{i+j}e(k-i) - b_{i+j-1}u_s(k-i+d-1)\} + \sum_{i=0}^{n-j}\Delta\rho_{i+j}(k-i), \qquad 2 \le j \le n. \quad (26)$$

Together with (25a) and (26), the following equation is achieved:

$$X(k) = JY(k) + \Delta J(e, u_s, r) \quad (27a)$$

where definitions are given in (27b)–(27e), shown at the bottom of the next page. Because the uncertainties $\Delta J_i (2 \le j \le n)$ are

a function of u_s, we must cope with them, i.e., from (27e) and (25c)

$$\begin{aligned}\Delta J_2(e,u_s,r) = &\{\Delta H H^p[A'(q^{-1})+\Delta A'(q^{-1})\}e(k)\\ &+(1-\Delta H H^p)\Delta A'(q^{-1})e_f(k)\\ &+[B'(q^{-1})+\Delta B'(q^{-1})]\Delta(u(k-d+1))\\ &+\Delta B'(q^{-1})u_s(k-d+1) \qquad (28a)\end{aligned}$$

where

$$\begin{aligned}\Delta A'(q^{-1}) &= \Delta a_2 q^{-1}+\cdots+\Delta a_n q^{-n+1}\\ A'(q^{-1}) &= a_2 q^{-1}+\cdots+a_n q^{-n+1} \qquad (28b)\\ \Delta B'(q^{-1}) &= \Delta b_1 q^{-1}+\cdots+\Delta b_{n-1} q^{-n+1}\\ B'(q^{-1}) &= b_1 q^{-1}+\cdots+b_{n-1} q^{-n+1}. \qquad (28c)\end{aligned}$$

Similarly, ΔJ_i for $i \geq 3$. For simplicity, those are omitted.

2) Stability of the Sliding Surface: Define the following sliding surface:

$$s(k) = \sum_{i=0}^{n_s} d_i e(k-i). \qquad (29)$$

Without loss of generality, one lets $d_0 = 1$. One can choose $d_i (1 \leq i \leq n_s)$ which satisfies the inequality $|d_i| < 1/n_s$. Then, this sufficient condition ensures that $s(k) = 0$ is Hurwitz. In general, $n_s \leq n_a$. Once the operating point (or system's trajectory) is on the sliding surface, it will approach the origin in a finite time. If the DVSC $u_s(k-d+1)$ guarantees that any initial error state deviation from the sliding surface is eventually driven to, and then maintained on it, then the system is asymptotically stable. The following episode is to derive a sufficient condition for the asymptotic tracking when the operating point is in the neighborhood of the sliding surface. Rewrite (29) as

$$E(k+1) = DE(k) + Qs(k) \qquad (30)$$

where

$$\begin{aligned}E(k) &= [e_1(k) \quad e_2(k) \quad \cdots \quad e_{n_s}(k)]^T\\ &= [e(k-1) \quad e(k-2) \quad \cdots \quad e(k-n_s)]^T \qquad (31)\end{aligned}$$

$$D = \begin{bmatrix} -d_1 & -d_2 & \cdot & \cdot & \cdot & -d_{n_s} \\ 1 & & & & & \\ & \cdot & & & & \\ & & \cdot & & & \\ & & & \cdot & & \\ & & & & 1 & 0 \end{bmatrix}$$

$$Q = \begin{bmatrix} 1 \\ 0 \\ \cdot \\ \cdot \\ \cdot \\ 0 \end{bmatrix}. \qquad (32)$$

Then, the solution of (30) is described as follows:

$$E(k) = D^{k-k_0}E(k_0) + \sum_{j=k_0}^{k-1} D^{k-1-j}Qs(j), \qquad k \geq k_0. \qquad (33)$$

Since the dynamics of (30) are stable, there exist two positive constants P_1 and P_2 such that

$$\|D^{k-k_0}\| \leq P_1 P_2^{k-k_0}, \qquad k \geq k_0 \qquad (34)$$

where

$$P_2 = \max_{1\leq i\leq n_s} R_e\{|\lambda_i[D]\} < 1. \qquad (35)$$

Before examining the stability for $s(k) \neq 0$, the following discrete-time Gronwall-Bellman Lemma is introduced [23].

Lemma 1: Let $\{r_1(k)\}$, $\{r_2(k)\}$ and $\{r_3(k)\}$ be the sequences of real numbers with $\{r_3(k)\} \geq 0$ for $k \geq k_0$. If $r_1(k) \leq r_2(k) + \Sigma_{j=k_0}^{k-1} r_1(j)r_3(j)$, for $k \geq k_0$ and $r_2(k) \leq r_m \ \forall k$, then $r_1(k) \leq r_m \ \Pi_{0<j<k}\,[1+r_3(j)]$.

The next theorem discusses the stability of (30) when $s(k) \neq 0$.

Theorem 1: If the dynamics (30) satisfy the inequality $|s(k)| < \alpha\|E(k)\|$ for $k \geq k_0$, where $0 < \alpha < (1-P_2)/P_1$, and its initial condition $E(k_0)$ is bounded, then $e(k) \to 0$ with a rate $P_2 + \alpha P_1$ as $k \geq k_0$.

Proof: See Appendix C.

$$Y(k) = [e(k) \quad \cdots \quad e(k-n+1) \quad u_s(k-d) \quad \cdots \quad u_s(k-n-d)]^T \qquad (27b)$$

$$J = \begin{bmatrix} 1 & 0 & \cdot & \cdot & \cdot & & 0 \\ 0 & -a_2 & \cdots & -a_n & b_1 & \cdots & b_{n-1} \\ \cdot & -a_3 \cdots & & -a_n & 0 & b_2 \cdots & 0 \\ \cdot & \cdot & & & \cdot & \cdot & \cdot \\ \cdot & \cdot & & & \cdot & \cdot & \cdot \\ & -a_{n-1} & -a_n & 0 \cdots & 0 & b_{n-2} \quad b_{n-1} & 0 \cdots \quad 0 \\ 0 & -a_n & 0 & \cdots & 0 & b_{n-1} \quad 0 & \cdots \quad 0 \end{bmatrix} \qquad (27c)$$

$$\Delta J_1(e,u_s,r) = -\Delta H H^p e(k) - (1-\Delta H H^p)e_f(k) \qquad (27d)$$

$$\Delta J_j(e,u_s,r) = \sum_{i=0}^{n-j} \Delta\rho_{i+j}(k-i-1), \qquad 2 \leq j \leq n. \qquad (27e)$$

Remark 3: According to the Cayley–Hamilton Theorem, the matrix D^{k-k_0} can be described as an $n_s \times n_s$ matrix. Furthermore, the values of P_1 and P_2 can be determined; hence, the value of α is achieved from the relation $0 < \alpha < (1-P_2/P_1)$.

3) VSC: The following assumptions are required for the derivation of the proposed control $u_s(k-d+1)$ in Theorem 2:

$$\begin{aligned}\text{A2:}\quad &\|(\overline{HG})^{-1}\{\Delta\beta + \Delta B'(q^{-1}) \\ &+ \mu_1[(\overline{H}+\Delta H)(\overline{G}+\Delta G) \\ &+ B'(q^{-1}) + \Delta B'(q^{-1})]\}\|_\infty \le \beta < 1 \end{aligned} \tag{36}$$

where

$$\Delta\beta = \overline{H}\Delta G + \Delta H[\overline{G}+\Delta G], \overline{HG} \neq 0 \tag{37a}$$

$$\|W(q^{-1})\|_\infty = \sup_{r\in(0,1)} \max_{0\le\theta\le 2\pi} |W(re^{-j\theta})|. \tag{37b}$$

The definition of (37b), e.g., can refer to Vidyasagar [24].

A3: The system uncertainties $K_u(k)$ caused by $\Delta F, \Delta G, \Delta H, \Delta(u)$ and $e_f(k)$ are described as follows:

$$\begin{aligned} K_u(k) &= \sum_{i=0}^{n_u} \kappa_i(k)\phi_i(k) \\ &\ge \{[\Delta H\overline{F} + \overline{H}\Delta F + \Delta H\Delta F]H^p \\ &\quad + \Delta H H^p[a_1 + A'(q^{-1}) + \Delta A'(q^{-1})] \\ &\quad - \Delta A'(q^{-1})\}e(k) \\ &\quad + \{\Delta\beta + \Delta B'(q^{-1}) + [(\overline{H}+\Delta H)(\overline{G}+\Delta G) \\ &\quad + B'(q^{-1}) + \Delta B'(q^{-1})]\mu_1\}u_{eq}(k-d+1) \\ &\quad + [(\overline{H}+\Delta H)(\overline{G}+\Delta G) \\ &\quad + B'(q^{-1}) + \Delta B'(q^{-1})]\mu_0 \\ &\quad + \{q - (\Delta H\overline{F} + \overline{H}\Delta F + \Delta H\Delta F)H^p \\ &\quad + (1 - \Delta H H^p)[a_1 + \Delta A'(q^{-1})]\}e_f(k) \end{aligned} \tag{38}$$

where

$$|\kappa_i(k)| < k_{\max} \quad \forall k, 0 \le i \le n_u = n_s + 3, \tag{39}$$

$$\begin{aligned} \phi_i(k) &= e(k-i), \qquad 0 \le i \le n_s, \\ \phi_{n_u-2}(k) &= u_{eq}(k-d+1), \quad \phi_{n_u-1}(k) = r(k+n_b), \\ \phi_{n_u}(k) &= 1. \end{aligned} \tag{40}$$

Theorem 2: Consider the system (23) and (24) and the following controller:

$$u_s(k-d+1) = u_{eq}(k-d+1) + u_{sw}(k-d+1) \tag{41}$$

where

$$u_{eq}(k-d+1) = -(\overline{HG})^{-1} \cdot \left[\overline{HF}JY(k) + \sum_{i=0}^{n_s}(d_{i+1}-d_i)e(k-i)\right] \tag{42}$$

$$\begin{aligned} u_{sw}(k-d+1) &= -(\overline{HG})^{-1}\sum_{i=0}^{n_u+1}\psi_i(k)\phi_i(k), \\ \phi_{n_u+1}(k) &= s(k) \end{aligned} \tag{43}$$

$$\psi_i(k) = \begin{cases} -\gamma(k)\ \text{sgn}\,[s(k)\phi_i(k) - \xi_i(k)]/(1-\beta), \\ \qquad \text{if } |s(k)\phi_i(k)| \ge \xi_i(k) \\ 0, \quad \text{otherwise} \end{cases} \tag{44}$$

$$\begin{aligned} \xi_i(k) &= [\gamma(k)/(1-\beta) + k_{\max}]^2|\phi_i(k)| \\ &\quad \cdot \sum_{j=0}^{n_u+1}|\phi_j(k)|/\{2[\gamma(k) - k_{\max}]\} > 0. \end{aligned} \tag{45}$$

Under the condition $|s(k)\phi_i(k)| \ge \xi_i(k)$, the amplitude of the switching gain $\psi_i(k)$ is achieved from the following inequality:

$$\gamma_2(k) > \gamma(k) > \max[k_{\max}, \gamma_1(k)] \ge 0 \tag{46}$$

where

$$\gamma_{1,2}(k) = \left[f_2(k) \pm \sqrt{f_2^2(k) - f_1(k)f_3(k)}\right]/f_1(k) \tag{47}$$

$$f_1(k) = \sum_{j=0}^{n_u+1}|\phi_j(k)|/(1-\beta)^2 \tag{48}$$

$$f_2(k) = |s(k)| - k_{\max}\sum_{j=0}^{n_u+1}|\phi_j(k)|/(1-\beta) > 0 \tag{49}$$

$$f_3(k) = 2k_{\max}|s(k)| + k_{\max}^2\sum_{j=0}^{n_u+1}|\phi_j(k)|. \tag{50}$$

The overall system satisfies the following conditions: 1) a stable sliding surface; 2) the inequality

$$\begin{aligned} |s(k)| &< \max_{0\le i\le n_u+1}\left\{2(2-\beta)k_{\max}\sum_{j=0}^{n_u+1}|\phi_j(k)|/\right. \\ &\qquad \left. \cdot (1-\beta)^2, \xi_i(k)/|\phi_i(k)|\right\} \\ &< \alpha\|E(k)\| \quad \text{for } k \ge k_0 \end{aligned}$$

and 3) the assumptions A1–A3. As the controller (41) is applied to the system (23) and (24), $\{u_s(k)\}$ is bounded and $e(k) \to 0$ with a rate $P_2 + \alpha P_1$ as $k \to \infty$.

Proof: See Appendix D.

Remark 4: For the smoothness of control input, the sgn$(\cdot)$ function in (44) is modified as $sat(\cdot)$ function described as follows:

$$\begin{aligned} &sat\{[s(k)\phi_i(k) - \xi_i(k)]/\lambda_i\} \\ &\quad = \begin{cases} \text{sgn}[s(k)\phi_i(k) - \xi_i(k)], \\ \qquad \text{as } [s(k)\phi_i(k) - \xi_i(k)]/\lambda_i > 1, \lambda_i > 0 \\ [s(k)\phi_i(k) - \xi_i(k)]/\lambda_i, \\ \qquad \text{otherwise.} \end{cases} \end{aligned} \tag{51}$$

V. Experimental Results

The sliding surface for the DVSC is selected as $s(k) = e(k) - 0.4e(k) + 0.04e(k-2)$. Consider the proposed piezomechanics with reference input $r(t) = 36\sin(2\pi ft)$ μm, where f denotes the frequency (hertz). The control cycle time of the following

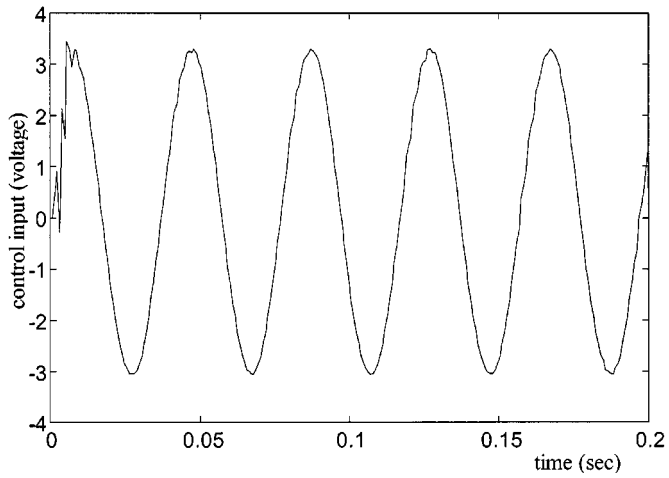

Fig. 7. Time history of control input $u(k)$ of IVSC for reference $36\sin(50\pi t)$ μm.

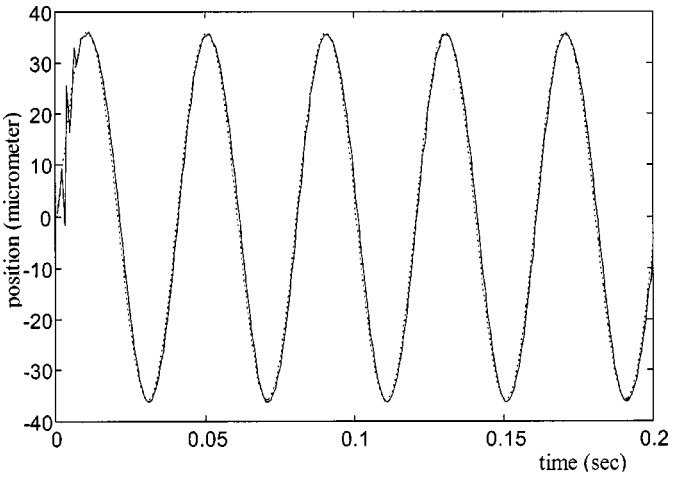

Fig. 8. Time history of output response $y(k)$ (—) of IVSC for reference $36\sin(50\pi t)$ μm $(\ldots)$.

experiments is set to be $T_c = 0.0008$ s, i.e., $t = 0.0008k, k = 0, 1, \cdots$. The hysteresis of the piezomechanics is canceled by the forward control (13) and (14). The control parameters of $u_{sw}(k-d+1)$ in DVSC are chosen as $\beta = 0.01$ and $k_{\max} = 0.001$ which are small enough because of the reduction of uncertainties by a forward control. Combined with the selection of boundary layer $\lambda_i = 0.1$ in (51), the control chattering does not appear. Fig. 7 shows that the control input of the reference input of 25 Hz is smooth. In fact, the control input for the other frequencies of reference input is also smooth. This is one of the features of the proposed control. It has reduced the uncertainties by using a forward control. Furthermore, its tracking ability is verified by Fig. 8 and Tables I and II. For demonstrating the effectiveness of the proposed methodology, the following PID controller [25, Ch. 8] is also employed for the piezomechanism:

$$\begin{aligned} u(k) = &(1+a_d)u(k-1) - a_d u(k-2) \\ &+ t_0 r(k) + t_1 r(k-1) + t_2 r(k-2) \\ &- s_0 y(k) - s_1 y(k-1) - s_2 y(k-2) \end{aligned} \quad (52a)$$

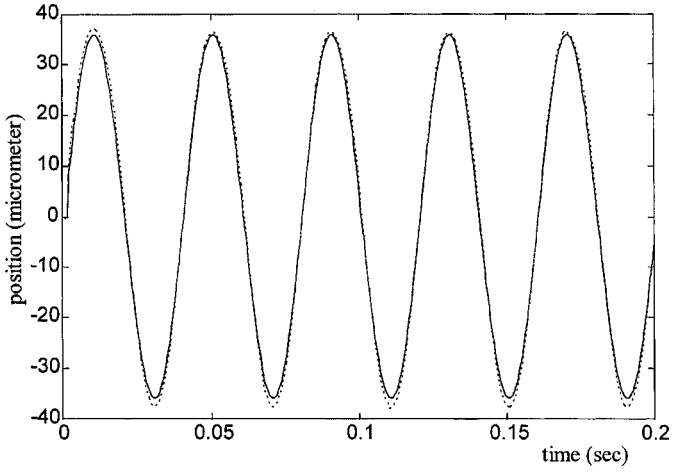

Fig. 9. Time history of output response of PID control $y(k)$ (—) for reference $36\sin(50\pi t)$ μm $(\ldots)$.

where

$$\begin{aligned} a_d &= (2T_d - NT_c)/(2T_d + NT_c) \\ b_d &= 2NT_d/(2T_d + NT_c) \\ b_i &= T_c/(2T_i) \end{aligned} \quad (52b)$$

$$\begin{aligned} t_0 &= k_p(b + b_i) \\ t_1 &= -k_p[b(1+a_d) - b_i(1-a_d)], \\ t_2 &= k_p a_d(b - b_i) \end{aligned} \quad (52c)$$

$$\begin{aligned} s_0 &= k_p(a_d + b_d + b_i a_d), \\ s_1 &= -k_p[1 + a_d + 2b_d - b_i(1-a_d)] \\ s_2 &= k_p(a_d + b_d - b_i a_d) \end{aligned} \quad (52d)$$

$$T_i = 3 \quad T_d = 20 \quad k_p = 0.1 \quad N = 3 \quad b = 15. \quad (52e)$$

The tracking response for 25 Hz resulting from the PID controller is shown in Fig. 9. According to the theory in [25], the value of b in (52e) should not be larger than one. However, if the control parameters are selected under this constraint, the tracking performance is poor [see Fig. 10(a)]. In addition, the output response for $k_p = 1.5$ is oscillatory [e.g., see Fig. 10(b)]. It not only has tracking error greater than that of the open-loop system, but also contains undesired high-frequency signals. To verify the effectiveness of the proposed IVSC control, an input signal is used as a reference signal. The tracking result for PID and IVSC are presented in Figs. 11 and 12. Comparing with Figs. 7–12 and Tables I and II, the following conclusions are drawn.

1) All control inputs are smooth.
2) After trial and- error and modification of the PID control, the tracking results are acceptable. For example, its maximum tracking error is about 6% of the amplitude of the reference input, which is the same as Ge and Jouaneh [10]. However, a reference input with the combination of different frequencies or amplitudes degrades its tracking performance (see Fig. 11).
3) Compared with various controllers, the proposed controller results in the smallest maximum tracking error for various frequencies.
4) Tracking error increases as the frequency of reference input increases.

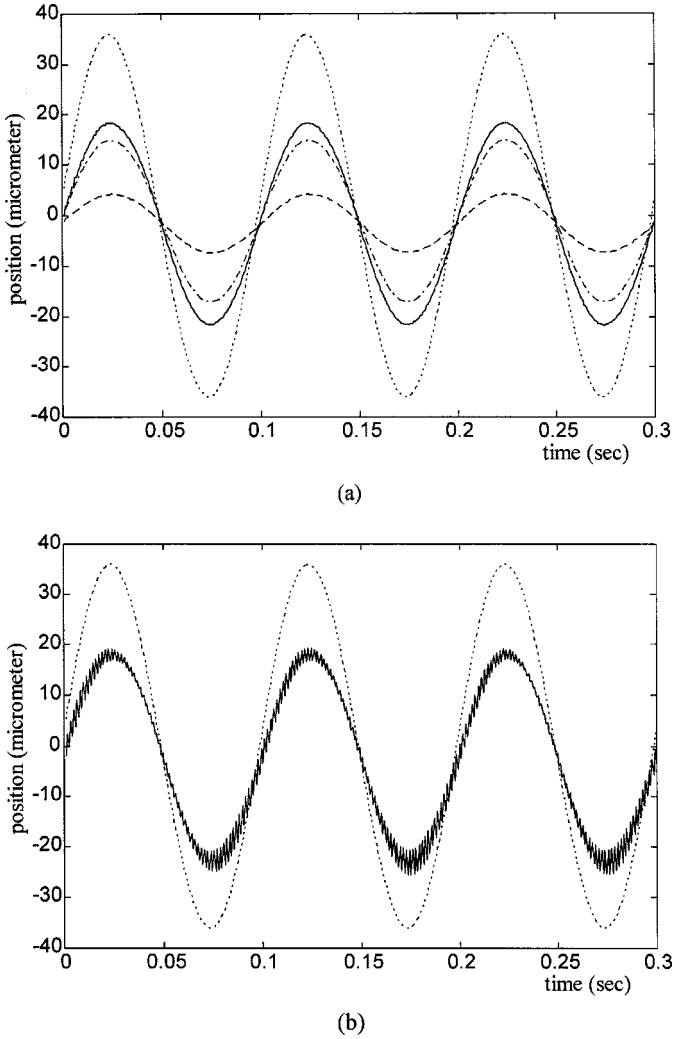

Fig. 10. Time histories of output response of PID control for reference $36\sin(30\pi t)$ μm $(\ldots)$ with b = 0.98, T_d = 2000, T_i = 0.000 01, N = 3, and different k_p. (a) k_p = 0.3 (- - -), k_p = 1 (-.-), k_p = 1.45(—). (b) k_p = 1.5 (—).

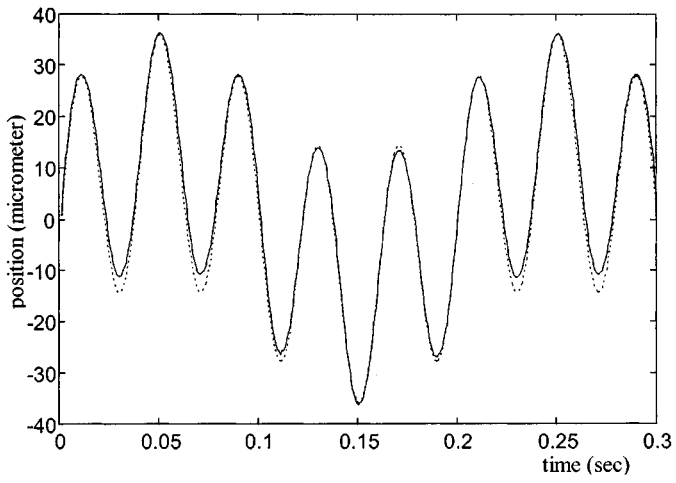

Fig. 11. Time histories of output response $y(k)$ (—) of PID control for reference $24\sin(50\pi t) + 12\sin(10\pi t)$ μm $(\ldots)$.

5) The closed-loop system including hardware and software with the proposed controller has the best improvement for the amplitude of frequency response. Similarly, the phase shift between input and output signal of the closed-loop system with the proposed controller is smaller than that of the open-loop system and the closed-loop system with PID controller.
6) There are no limitations for tracking cyclic reference signals, such as sinusoidal or triangular signals [10].
7) No state estimator is required for the proposed control; this feature enables the control system to be more practical in implementation [17].
8) If the input signal of 15 Hz is used to achieve the mathematical model, the tracking performance is better for the reference near 15 Hz. The result is given in Table I.

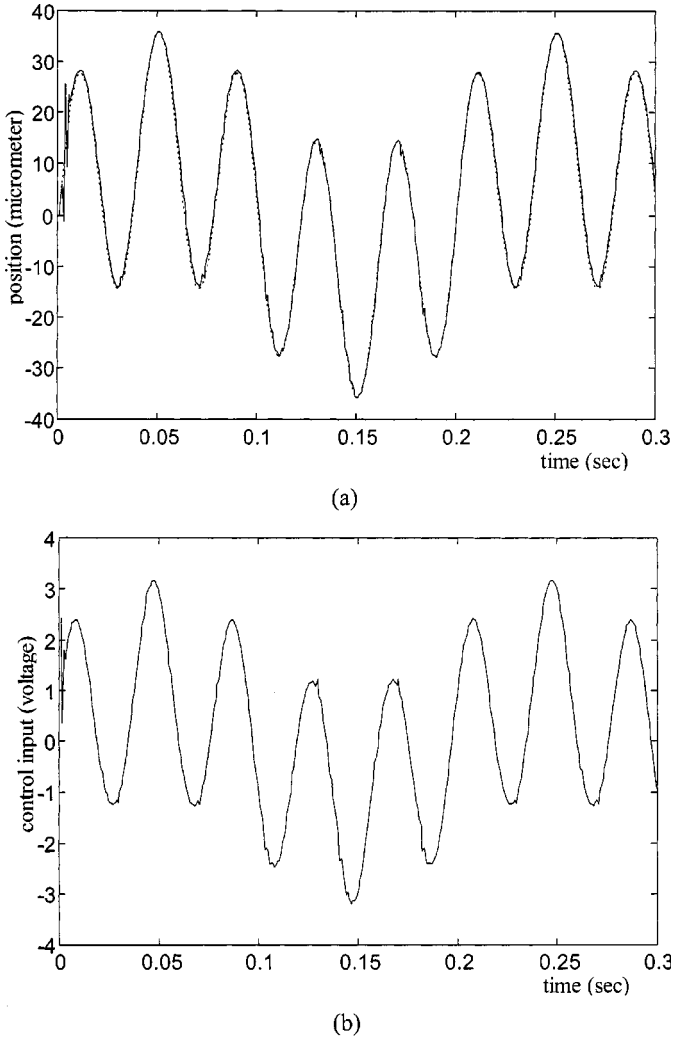

Fig. 12. Time histories of IVSC for reference $24\sin(50\pi t) + 12\sin(10\pi t)$ μm $(\ldots)$ (a) System output $y(k)$ (—). (b) Control input $u(k)$.

VI. Concluding Remarks

Piezomechanics were developed by an IVSC including a theoretical study and an experimental verification. The maximum tracking error by using hardware is over 14% of the amplitude of reference input that is not adequate for a precise positioning. Although a PID controller can accomplish an accept-

able tracking result, its maximum tracking error is over 6% [10]. The proposed controller for the same case results in a maximum tracking error smaller than 2.2% and a maximum phase shift between input and output signals smaller than 2°. The reasons for these results can be attributed to the following factors.

1) A novel forward control is applied to cancel the effect of hysteresis and to track a reference input in a satisfactory manner.
2) An effective DVSC is then employed to improve the system performance including accuracy of trajectory tracking and smoothness of control input.
3) No state estimator is required for the proposed controller.

Due to these advantages, the proposed methodology is an "intelligent" VSC for piezomechanics. Further work will be to use the proposed piezomechanics for noncircular grinding [12], [26].

APPENDIX A

The partial differentials are described as follows:

$$\begin{aligned}\frac{\partial J(k)}{\partial c_1(k-1)} &= \frac{\partial J(k)}{\partial y_n(k)}\,\frac{\partial y_n(k)}{\partial c_1(k-1)} \\ &= \frac{-\lfloor y_p(k)-y_n(k)\rfloor}{c_1^2(k-1)\{1+z(k-1)\}^2} b_1(k-1) \\ &\quad \cdot \{4c_1(k-1)[u(k-1)-c_2(k-1)]z(k-1) \\ &\quad + z(k-1)^2 + 2c_1^2(k-1)c_3(k-1) \\ &\quad \cdot [u(k-1)-c_2(k-1)]z(k-1)-1\} \end{aligned} \tag{A1}$$

$$\begin{aligned}\frac{\partial J(k)}{\partial c_2(k-1)} &= \frac{\partial J(k)}{\partial y_n(k)}\,\frac{\partial y_n(k)}{\partial c_2(k-1)} \\ &= 2[y_p(k)-y_n(k)]b_1(k-1)z(k-1) \\ &\quad \cdot [2+c_1(k-1)c_3(k-1)]/\{1+z(k-1)\}^2 \end{aligned} \tag{A2}$$

$$\begin{aligned}\frac{\partial J(k)}{\partial c_3(k-1)} &= \frac{\partial J(k)}{\partial y_n(k)}\,\frac{\partial y_n(k)}{\partial c_3(k-1)} \\ &= -[y_p(k)-y_n(k)]b_1(k-1)/[1+z(k-1)] \end{aligned} \tag{A3}$$

$$\begin{aligned}\frac{\partial J(k)}{\partial a_i(k-1)} &= \frac{\partial J(k)}{\partial y_n(k)}\,\frac{\partial y_n(k)}{\partial a_i(k-1)} \\ &= [y_p(k)-y_n(k)]y_n(k-i), \qquad 1\le i\le m \end{aligned} \tag{A4}$$

$$\begin{aligned}\frac{\partial J(k)}{\partial b_i(k-1)} &= \frac{\partial J(k)}{\partial y_n(k)}\,\frac{\partial y_n(k)}{\partial b_i(k-1)} \\ &= -[y_p(k)-y_n(k)]v(k-i), \qquad 1\le i\le m. \end{aligned} \tag{A5}$$

The time-varying gains are selected as follows:

$$\alpha_i(e_r) = \delta_i\{1-e^{-\tau_i[y_n(k)-y_p(k)]^2}\}, \qquad \delta_i,\tau_i > 0 \tag{A6}$$

$$\beta_i(e_r) = \rho_i\{1-e^{-\chi_i[y_n(k)-y_p(k)]^2}\}, \qquad \rho_i,\chi_i > 0 \tag{A7}$$

$$\gamma_i(e_r) = \zeta_i\{1-e^{-\upsilon_i[y_n(k)-y_p(k)]^2}\}, \qquad \zeta_i,\upsilon_i > 0. \tag{A8}$$

Q.E.D.

APPENDIX B

The coefficients of the learned neural network are described as follows:

$$\begin{aligned}&\bar{a}_1 = 0.303\,147 \quad \bar{a}_2 = 0.283\,635 \quad \bar{a}_3 = 0.175\,854 \\ &\bar{b}_1 = 1.225\,019 \quad \bar{b}_2 = -0.498\,813 \quad \bar{b}_3 = 0.933\,584 \\ &\bar{c}_{1p} = -0.015\,012 \quad \bar{c}_{2p} = 0.775\,711 \quad \bar{c}_{3p} = 1.491\,532 \\ &\bar{c}_{1n} = -0.110\,386 \quad \bar{c}_{2n} = -0.258\,880 \quad \bar{c}_{3n} = -0.482\,705. \end{aligned}$$

Q.E.D.

APPENDIX C
PROOF OF THEOREM 1

Taking the norm of (33) and using the inequality $|s(k)| < \alpha\|E(k)\|$ result in

$$\|E(k)\| \le p_1 P_2^{k-k_0}\|E(k_0)\| + \alpha P_1 \sum_{j=k_0}^{k-1} P_2^{k-1-j}\|E(j)\|. \tag{C1}$$

Multiplying $P_2^{-(k-k_0)}$ on both sides of (C1) yields

$$\begin{aligned}P_2^{-(k-k_0)}\|E(k)\| &\le P_1\|E(k_0)\| \\ &\quad + \frac{\alpha P_1}{P_2}\sum_{j=k_0}^{k-1} P_2^{-(j-k_0)}\|E(j)\|. \end{aligned} \tag{C2}$$

Using the result of *Lemma 1* shows

$$\begin{aligned}&P_2^{-(k-k_0)}\|E(k)\| \\ &\qquad \le P_1\|E(k_0)\|\left(1+\frac{\alpha P_1}{P_2}\right)^{k-k_0}, \quad \text{for } k\ge k_0 \text{ or} \\ &\|E(k)\| \le P_1\|E(k_0)\|(P_2+\alpha P_1)^{k-k_0}, \qquad k\ge k_0. \end{aligned} \tag{C3}$$

Because $0 < \alpha < (1-P_2)/P_1$ and $\|E(k_0)\|$ is bounded, $\|E(k)\|$ (or $|e(k)|$) $\to 0$ with a rate $P_2+\alpha P_1$ as $k\to\infty$.Q.E.D.

APPENDIX D
PROOF OF THEOREM 2

Define the following Lyapunov function:

$$V[s(k)] = s^2(k)/2 > 0, \qquad \text{for } s(k)\ne 0. \tag{D1}$$

Then, the change rate of the Lyapunov function is expressed as follows:

$$\Delta V(k) = V[s(k+1)] - V[s(k)] = s(k)\Delta s(k) + \Delta s^2(k)/2 \tag{D2}$$

where $\Delta s(k) = s(k+1) - s(k)$. The following can be demonstrated:

$$\begin{aligned}
\Delta s(k) &= \sum_{i=0}^{n_s} d_i[e(k-i+1) - e(k-i)], \quad \text{using (29)} \\
&= [\overline{H} + \Delta H(k)]\{[\overline{F} + \Delta F(k)]X(k) \\
&\quad + [\overline{G} + \Delta G(k)][u_s(k-d+1) \\
&\quad + \Delta(u(k-d+1))]\} \\
&\quad + \sum_{i=0}^{n_s} (d_{i+1} - d_i)e(k-i) + e_f(k+1), \\
&\quad \text{using (22) and (23)} \\
&= \overline{HF}JY(k) + \overline{HG}u_s(k-d+1) \\
&\quad + \sum_{i=0}^{n_s} (d_{i+1} - d_i)e(k-i) \\
&\quad + [\Delta H\overline{F} + \overline{H}\Delta F + \Delta H\Delta F]X(k) \\
&\quad + (\overline{H} + \Delta H)(\overline{G} + \Delta G)\Delta(u(k-d+1)) \\
&\quad + \Delta\beta u_{eq}(k-d+1) + \Delta\beta u_{sw}(k-d+1) \\
&\quad - a_1\Delta J_1(e, u_s, r) + \Delta J_2(e, u_s, r) + e_f(k+1) \\
&\le \{\overline{HG} + \Delta\beta + \Delta B'(q^{-1}) \\
&\quad + \mu_1[(\overline{H} + \Delta H)(\overline{G} + \Delta G) \\
&\quad + B'(q^{-1}) + \Delta B'(q^{-1})]\}u_{sw}(k-d+1) \\
&\quad + K_u(k) \quad \text{using assumptions A1–A3, (23),} \\
&\quad \text{(25d), (27a), (28a), (38), and (42)} \\
&= \sum_{i=0}^{n_u+1} [\eta(k)\psi_i(k) + \kappa_i(k)]\phi_i(k) \quad \text{using (38) and (43)}
\end{aligned} \tag{D3}$$

where

$$\begin{aligned}
\eta(k) = 1 &+ (\overline{HG})^{-1}\{\Delta\beta + \Delta B'(q^{-1}) \\
&+ \mu_1[(\overline{H} + H)(\overline{G} + G) \\
&+ B'(q^{-1}) + \Delta B'(q^{-1})]\}, \qquad \kappa_{n_u+1} = 0.
\end{aligned} \tag{D4}$$

To make $\Delta V(k) \le -\zeta V(k)$, where $0 < \zeta < 1$, the following equation is achieved:

$$\begin{aligned}
\Delta\overline{V}(k) = s(k)&\left\{\sum_{i=0}^{n_u+1} [\eta(k)\psi_i(k) + \kappa_i(k)]\phi_i(k)\right\} \\
&+ \Delta s^2(k)/2 \le 0
\end{aligned} \tag{D5}$$

where $\kappa_{n_u+1} = \zeta/2 < k_{\max}$. Consider the following two cases.

1) If $|s(k)\phi_i(k)| \ge \xi_i(k)$,

$$\begin{aligned}
\Delta\overline{V}(k) &\le -\sum_{i=0}^{n_u+1} \{\eta(k)\gamma(k)/(1-\beta) - k_{\max}\}\xi_i(k) \\
&\quad + \Delta s^2(k)/2 \\
&< -\sum_{i=0}^{n_u+1} [\gamma(k) - k_{\max}]\xi_i(k) + \Delta s^2(k)/2, \\
&\quad \text{using using (D4), (36),} \\
&= -\sum_{i=0}^{n_u+1} [\gamma(k)/(1-\beta) + k_{\max}]|\phi_i(k)| \\
&\quad \cdot \sum_{j=0}^{n_u+1} [\gamma(k)/(1-\beta) + k_{\max}]|\phi_j(k)|/2 + \Delta s^2(k)/2 \\
&\le 0 \quad \text{using (45) (D3), (D4), (29), and (40).}
\end{aligned} \tag{D6}$$

According to Lyapunov theory, if the condition $|s(k)\phi_i(k)| \ge \xi_i(k)$ is satisfied, the signal $s(k)$ continuously decreases. Furthermore, the amplitude of $\psi_i(k)$ achieved from the condition $|s(k)\phi_i(k)| \ge \xi_i(k)$ is described as follows:

$$f_1(k)\gamma^2(k) - 2f_2(k)\gamma(k) + f_3(k) \le 0. \tag{D7}$$

Because $\xi_i(k) > 0$ and the assumptions of $f_2(k) > 0$ (i.e., $|s(k)| > k_{\max} \sum_{j=0}^{n_u+1} |\phi_j(k)|/(1-\beta)$) and $f_2^2(k) - f_1(k)f_3(k) > 0$ (i.e., $|s(k)| > 2(2-\beta)k_{\max} \sum_{j=0}^{n_u+1} |\phi_j(k)|/(1-\beta)^2$), the result (46) is obtained. Furthermore, $|s(k)| < \max_{0\le i\le n_u+1}\{2(2-\beta)k_{\max} \sum_{j=0}^{n_u+1} |\phi_j(k)|/(1-\beta)^2, \xi_i(k)/|\phi_i(k)|\} < S_{in}$ is an invariant set.

2) If $|s(k)\phi_i(k)| < \xi_i(k)$ or $f_2(k) < 0$ or $f_2^2(k) - f_1(k)f_3(k) < 0$, then $\psi_i(k) = 0$. Under this situation, $|s(k)| < \max_{0\le i\le n_u+1}\{2(2-\beta)k_{\max} \sum_{j=0}^{n_u+1} |\phi_j(k)|/(1-\beta)^2, \xi_i(k)/|\phi_i(k)|\} < S_{in}$ is also an invariant set. Based on the result of Theorem 1, the condition $|s(k)| < \max_{0\le i\le n_u+1}\{2(2-\beta)k_{\max} \sum_{j=0}^{n_u+1} |\phi_j(k)|/(1-\beta)^2, \xi_i(k)/|\phi_i(k)|\} < \alpha\|E(k)\|$ for any $k \ge k_0$ is satisfied, the $e(k) \to 0$ with a rate $P_2 + \alpha P_1$ as $k \to \infty$. Q.E.D.

REFERENCES

[1] J. Stroscio and W. Kaiser, *Scanning Tunneling Microscopy*. New York: Academic, 1993.

[2] A. B. Palazzolo, S. Jagannathan, A. F. Kascak, G. T. Montague, and L. J. Kiraly, "Hybrid active vibration control of rotor bearing systems using piezoelectric actuators," *Trans. ASME, J. Vib. Acoust.*, vol. 115, pp. 111–119, 1993.

[3] Y. Okazaki, "A micro-positioning tool post using piezoelectric actuator for diamond turning machines," *Precis. Eng.*, vol. 12, no. 3, pp. 151–156, 1990.

[4] J. D. Kim and S. R. Nam, "Developent of a micro-positioning grinding table using piezoelectric voltage feedback," *Proc. Inst. Mech. Eng.—I, J. Syst. Control Eng.*, vol. 209, pp. 469–474, 1995.

[5] K. Bansevicius, R. Parkin, A. Jebb, and J. Knight, "Piezomechanics as a subsystem of mechatronics: Present state of art, problems, future developments," *IEEE Trans. Ind. Electron.*, vol. 43, pp. 23–29, Feb. 1996.

[6] H. R. Pota and T. E. Alberts, "Multivariable transfer functions for a slewing piezoelectric laminate beam," *Trans. ASME, J. Dyn. Syst. Meas. Control*, vol. 117, pp. 352–359, 1995.
[7] C. J. Li, H. S. M. Beigi, S. Li, and J. Liang, "Nonlinear piezo-actuator control by learning self-tuning regulator," *Trans. ASME, J. Dyn. Syst. Meas. Control*, vol. 115, pp. 720–723, 1993.
[8] S. B. Jung and S. W. Kim, "Improvement of scanning accuracy of PZT piezoelectric actuator by feed-forward model-reference control," *Precis. Eng.*, vol. 16, no. 1, pp. 49–55, 1994.
[9] T. Gang and P. V. Kokotovic, "Adaptive control of plants with unknown hysteresis," *IEEE Trans. Automat. Contr.*, vol. 40, pp. 200–212, Feb. 1995.
[10] P. Ge and M. Jouaneh, "Tracking control of a piezoceramic actuator," *IEEE Trans. Contr. Syst. Technol.*, vol. 4, pp. 209–216, May 1996.
[11] J. M. T. A. Adrians, W. L. de Koning, and R. Banning, "Design and modeling of a piezo-actuator positioning mechanism," in *Proc. 36th IEEE CDC*, San Diego, CA, Dec. 10–12, 1997, pp. 1978–1983.
[12] C. L. Hwang, M. H. Wei, and W. J. Jieng, "Noncircular cutting with a lathe using a three-stage intelligent controller," *Robot. Comput.-Integr. Manuf.*, vol. 13, no. 3, pp. 181–191, 1997.
[13] V. I. Utkin, "Variable structure with sliding modes," *IEEE Trans. Automat. Contr.*, vol. 22, pp. 212–222, Feb. 1977.
[14] J.-J. E. Slotine and J. A. Coestsee, "Adaptive sliding controller synthesis for nonlinear systems," *Int. J. Control*, vol. 43, no. 6, pp. 1631–1651, 1986.
[15] C. L. Hwang, "Design of servocontroller via the sliding mode technique," *Proc. IEE—Control Theory Applicat.*, pt. D, vol. 139, no. 5, pp. 439–446, 1992.
[16] K. Furuta, "VSS type self-tuning control," *IEEE Trans. Ind. Electron.*, vol. 40, pp. 37–44, Feb. 1993.
[17] R. El-Khazali and R. A. DeCarlo, "Output feedback variable structure control design," *Automatica*, vol. 31, no. 6, pp. 805–816, 1995.
[18] C. L. Hwang, "Sliding mode control using time-varying switching gain and boundary layer for electrohydraulic position and differential pressure control," *Proc. IEE—Control Theory Applicat.*, pt. D, vol. 143, no. 4, pp. 325–332, 1996.
[19] P. Kachroo and M. Tomizuka, "Chattering reduction and error convergence in the sliding-mode control of a class of nonlinear systems," *IEEE Trans. Automat. Contr.*, vol. 41, pp. 1063–1068, July 1997.
[20] P. Korondi, H. Hashimoto, and V. Utkin, "Direct control of flexible shaft in an observer-based discrete-time sliding mode," *IEEE Trans. Ind. Electron.*, vol. 45, pp. 291–296, Apr. 1998.
[21] P. M. Lee and J. H. Oh, "Improvement on VSS-type self-tuning control for a tracking controller," *IEEE Trans. Ind. Electron.*, vol. 45, pp. 319–325, Apr. 1998.
[22] O. Kaynak and A. Sabanovic, "A study on robustness property of sliding-mode controllers: A novel design and experimental investigations," *IEEE Trans. Ind. Electron.*, vol. 46, pp. 1012–1018, Oct. 1999.
[23] C. A. Desoer and M. Vidyasagar, *Feedback System: Input-Output Properties*. New York: Academic, 1975.
[24] M. Vidyasagar, *Optimal Control System Synthesis*. Englewood Cliffs, NJ: Prentice-Hall, 1986.
[25] K. J. Astrom and B. Wittenmark, *Computer-Controlled Systems—Theory and Design*, 2nd ed. Englewood Cliffs, NJ: Prentice-Hall, 1990.
[26] A. Frank and A. Schmid, "Grinding of noncircular contours on CNC cylindrical grinding machines," *Robot. Comput.-Integr. Manuf.*, vol. 4, no. 3, pp. 211–218, 1988.

Chih-Lyang Hwang received the B.E. degree in aeronautical engineering from Tamkang University, Taipei, Taiwan, R.O.C., and the M.E. and Ph.D. degrees in mechanical engineering from Tatung Institute of Technology, Taipei, Taiwan, R.O.C., in 1981, 1986, and 1990, respectively.

Since 1990, he has been with the Department of Mechanical Engineering, Tatung Institute of Technology, where he is engaged in teaching and research in the areas of servo control and control of manufacturing systems. Since 1996, he has been a Professor of Mechanical Engineering. In 1998–1999, he was a Research Scholar in the George W. Woodruff School of Mechanical Engineering, Georgia Institute of Technology, Atlanta. He has authored or coauthored about 50 journal and conference papers. His current research interests include neural-network modeling and control, variable-structure control, fuzzy control, mechatronics, and robotics.

Prof. Hwang has received a number of awards, including the Excellent Research Paper Award from the National Science Council of Taiwan and Hsieh-Chih Industry Renaissance Association of Tatung Company.

Chau Jan was born in Taiwan, R.O.C., in 1972. He received the B.E. degree in 1996 from the Department of Mechanical Engineering, National Cheng Kung University, Tainan, Taiwan, R.O.C., and the M.E. degree in mechanical engineering in 1998 from Tatung University, Taipei, Taiwan, R.O.C.. where he is currently working toward the Ph.D. degree in mechanical engineering.

His current research interests include control systems, robust control, neural networks, fuzzy systems, and piezomechanics.

Ye-Hwa Chen received the B.S. degree in chemical engineering from National Taiwan University, Taipei, Taiwan, R.O.C., and the M.S. and Ph.D. degrees in mechanical engineering from the University of California, Berkeley, in 1979, 1983, and 1985, respectively.

From 1986 to 1988, he was with the Department of Mechanical and Aerospace Engineering, Syracuse University, Syracuse, NY. Since 1988, he has been with the G.W. Woodruff School of Mechanical Engineering, Georgia Institute of Technology, Atlanta. He served as the Program Committee Chair for Mechatronics 2000, the 7th Mechatronics Forum International Conference and Mechatronics Education Workshop. He currently serves as an Associate Editor of *Intelligent Automation and Soft Computing: An International Journal*. His research interests include neural networks, fuzzy logic theory, control theory, and dynamic systems.

Dr. Chen has received a number of awards, including the Sigma Xi Junior Faculty Award and the Sigma Xi Best Research Paper Award. He is a member of the Amercian Society of Mechanical Engineers.